Phonon density of states of Sn in textured SnO under high pressure: Comparison of nuclear inelastic x-ray scattering spectra to a shell model

H. Giefers,[1,2,*] S. Koval,[3] G. Wortmann,[1] W. Sturhahn,[4] E. E. Alp,[4] and M. Y. Hu[5]
[1]*Department Physik, Universität Paderborn, D-33095 Paderborn, Germany*
[2]*Department of Physics, University of Nevada Las Vegas, Las Vegas, Nevada 89109, USA*
[3]*Instituto de Física Rosario, Universidad Nacional de Rosario, 27 de Febrero 210 Bis, 2000 Rosario, Argentina*
[4]*APS, Argonne National Laboratory, Argonne, Illinois 60439, USA*
[5]*HP-CAT, Carnegie Institute of Washington, APS, Argonne, Illinois 60439, USA*
(Received 8 May 2006; published 29 September 2006)

The local phonon density of states (DOS) at the Sn site in tin monoxide (SnO) is studied at pressures up to 8 GPa with ^{119}Sn nuclear resonant inelastic x-ray scattering (NRIXS) of synchrotron radiation at 23.88 keV. The preferred orientation (texture) of the SnO crystallites in the investigated samples is used to measure NRIXS spectra preferentially parallel and almost perpendicular to the *c* axis of tetragonal SnO. A subtraction method is applied to these NRIXS spectra to produce projected local Sn DOS spectra as seen parallel and perpendicular to the *c* axis of SnO. These experimentally obtained local Sn DOS spectra, both in the polycrystalline case as well as projected parallel and perpendicular to the *c* axis, are compared with corresponding theoretical phonon DOS spectra, derived from dispersion relations calculated with a recently developed shell model. Comparison between the experimental projected Sn DOS spectra and the corresponding theoretical DOS spectra enables us to follow the pressure-induced shifts of several acoustic and optic phonon modes. While the principal spectral features of the experimental and theoretical phonon DOS agree well at energies above 10 meV, the pressure behavior of the low-energy part of the DOS is not well reproduced by the theoretical calculations. In fact, they exhibit, in contrast to the experimental data, a dramatic softening of two low-energy modes, their energies approaching zero around 2.5 GPa, clearly indicating the limitations of the applied shell model. These difficulties are obviously connected with the complex Sn-O and Sn-Sn bindings within and between the Sn-O-Sn layers in the litharge structure of SnO. We derived from the experimental and theoretical DOS spectra a variety of elastic and thermodynamic parameters of the Sn sublattice, such as the Lamb-Mössbauer factor, the mean force constant, and Debye temperatures, as well as the vibrational contributions to the Helmholtz free energy, specific heat, entropy, and internal energy. We found, in part, good agreement between these values, for instance, for the Grüneisen parameters for some selected phonon modes, especially for some optical modes studied recently by Raman spectroscopy. We discuss in detail a possible anisotropy in the elastic parameters resulting from the litharge-type structure of SnO, for instance for the Lamb-Mössbauer factor, where we can compare with existing data from ^{119}Sn-Mössbauer spectroscopy.

DOI: 10.1103/PhysRevB.74.094303 PACS number(s): 63.20.Dj, 62.50.+p, 65.40.−b, 82.80.Ej

I. INTRODUCTION

Due to its technological applications, tin monoxide (SnO) has received much attention. Powders of SnO can be used as anode materials in lithium rechargeable batteries, as coating materials, or as effective catalysts for several acids.[1] SnO has the litharge-type (α-PbO) structure ($tP4$, $P4/nmm$, SG No. 129, $Z=2$). The structural parameters at ambient conditions are $a=3.800(2)$ Å, $c=4.836(2)$ Å (Refs. 2 and 3), and $z=0.2369$ (Ref. 4). This structure is formed by Sn-O -Sn layers stacked along the *c* direction with relatively weak van der Waals-type interactions[4] between the Sn-O-Sn layers (Fig. 1).

SnO is metastable at ambient conditions and above a certain temperature ($\approx$600 K) it decomposes by a disproportionation reaction with a noticeable rate to Sn and SnO_2. This decomposition was studied at ambient pressure[5] and under high pressure[6] with energy-dispersive x-ray diffraction (EDXRD). Only at ambient pressure the intermediate tin oxide Sn_2O_3 is found in the decomposition reaction. Besides the tetragonal SnO, two other metastable structures of SnO are known.[7,8]

Due to the platelike morphology of the SnO crystallites, Mössbauer spectra[9–11] or x-ray diffraction spectra[3] reveal a preferred orientation (texture) in the SnO samples. The *c* axis is preferentially oriented perpendicular to the substrate plane.

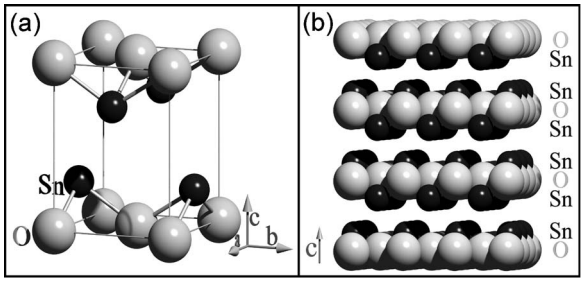

FIG. 1. (a) Unit cell of SnO in the litharge-type structure. Sn^{2+} (small black spheres) occupies the 2*c* site $(0,\frac{1}{2},z)$, O^{2-} (large white spheres) occupies the 2*a* site (0,0,0). (b) A $3\times3\times3$ super cell of SnO with spheres with the actual sizes of the Sn^{2+} and O^{2-} ions (0.93 Å and 1.32 Å, respectively) showing the layered structure of SnO and the wide-stretched open space between the Sn-O-Sn layers.

Recent high pressure studies under quasihydrostatic conditions reveal that SnO shows no structural phase transition up to 50 GPa.[2,3,12] The former observed tetragonal to orthorhombic phase transition[13,14] is caused by nonhydrostatic conditions due to the used pressure-transmitting media. The free positional parameter z of the Sn atoms under pressure was investigated by a combined extended x-ray-absorption fine structure (EXAFS) and EDXRD study[2] as well as by angle dispersive x-ray diffraction.[12] Infrared reflectivity measurements[12] indicate a semiconductor to metal transition in SnO at a pressure around 5 GPa. In high-pressure Raman spectra,[12] two strong optical zone-center modes ($E_g^{(1)}$, A_{1g}) could be identified. The pressure dependences of these modes reveal mode-Grüneisen parameters smaller than one. Very recently, first-principles electronic structure calculations were also performed to study the influence of pressure on the structural parameters, on the electronic bands, and also on a few zone-center phonon modes in SnO.[15] These calculations reveal that the indirect minimal gap closes around 5 GPa, in accordance with the above-mentioned infrared reflectivity data. The theoretical pressure dependence of the frequencies of the above Raman modes[12] is found to agree rather well for the $E_g^{(1)}$ mode, but differ significantly for the A_{1g} mode.

A comprehensive study of the lattice dynamics in SnO was performed previously by *ab initio* and shell-model calculations.[16,17] The zone-center phonon frequencies were computed by *ab initio* linear augmented-plane-wave (LAPW) frozen-phonon calculations, and a shell model was derived by fitting this data and the experimentally available Γ-phonon modes. Also, the specific heat data could be well described by the derived phonon DOS.[17] This recently developed shell model[17] is a refinement of a previous one that was used to obtain the partial phonon densities of states (DOS) for Sn and O, although these data could not be compared in detail with the experimental data due to the lack of partial phonon DOS data at that time.[16] Comparison was only possible with the Lamb-Mössbauer factor f_{LM} as a function of temperature by the integration of the partial Sn phonon DOS with the respective energy weighting, resulting in good agreement with experiment.[16,17]

In this work, we performed experimental and theoretical studies of the partial DOS of the Sn site in SnO as a function of pressure. To this purpose, we measured the phonon DOS at the Sn site using the technique of nuclear resonant inelastic x-ray scattering (NRIXS).[18–20] We also compared the experimental data with theoretical calculations using the improved version of the shell model.[17]

In pioneering experiments, it was demonstrated in 1995 with the ^{57}Fe(14.413 keV)-Mössbauer resonance that NRIXS of synchrotron radiation (SR) offers a unique way to study the local phonon DOS in compounds.[18,19] The first high-pressure studies using NRIXS were performed in 1999 with the ^{57}Fe-resonance on pure Fe.[21,22] The texture of ε iron in a diamond anvil cell (DAC) was used to investigate the orientation-dependent local Fe-phonon DOS along and perpendicular to the c axis in hexagonal iron.[23,24] The first NRIXS studies with the ^{119}Sn(23.88 keV)-Mössbauer resonance were published in 1998/99.[25,26] Here we present a high-pressure ^{119}Sn-NRIXS study applied to SnO using the

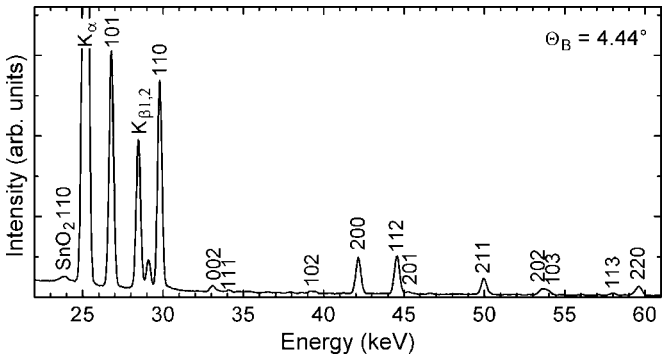

FIG. 2. EDXRD spectra of SnO which is 90% enriched in ^{119}Sn. The diffraction lines (hkl) of SnO and of the spurious SnO_2 contamination are indicated. The diffraction angle Θ_B was 4.44°. The strong difference between the intensities of the diffraction lines (110) and (002) reveals the strong texture of this sample (see also Ref. 3).

Paderborn-type DAC.[23] Employing the pressure-induced texture in the SnO sample, we were able to study the orientation-dependent phonon DOS of the Sn sublattice under pressures up to 6 GPa. From the derived Sn phonon DOS spectra, we analyzed the dependence of various elastic and thermodynamic properties as a function of pressure as well as of the crystalline orientation. The experimentally obtained Grüneisen parameters of some selected modes are compared with our shell-model calculations and with data from Raman experiments[12] as well as recent electronic structure calculations.[15]

The paper is organized as follows: In Sec. II we explain and give details of the experiments and the model calculations performed. In Sec. III we present and analyze the present results on SnO in three sections: In Sec. III A we present the experimental and theoretical results and compare them for polycrystalline SnO and derive and compare in Sec. III B the elastic and thermodynamic parameters. In Sec. III C, we evaluate the projected phonon DOS as seen parallel and perpendicular to the tetragonal c axis of SnO, use these projected phonon DOS for a mode-specific analysis of the data, derive the Grüneisen parameters for some of these modes, and compare them with Raman and *ab initio* data. In Sec. IV we present the conclusions. In the Appendix we describe the subtraction method used to derive projected local phonon DOS spectra from measured NRIXS spectra.

II. EXPERIMENTAL AND THEORETICAL DETAILS

Polycrystalline SnO was prepared by chemical reduction of SnO_2 which was enriched to 90% in ^{119}Sn. The present sample was also used in former nuclear resonant scattering experiments.[27] ^{119}Sn-Mössbauer spectra[27] and EDXRD spectra of this sample (Fig. 2) reveal a small contribution from unreduced SnO_2 of approximately 2%. Metallic tin could not be detected within the EDXRD spectra.

The high-pressure NRIXS experiments were performed with special designed diamond anvil cells (DAC).[23] With this DAC, the NRIXS spectra can be recorded with the incident synchrotron radiation parallel (0° geometry) or almost

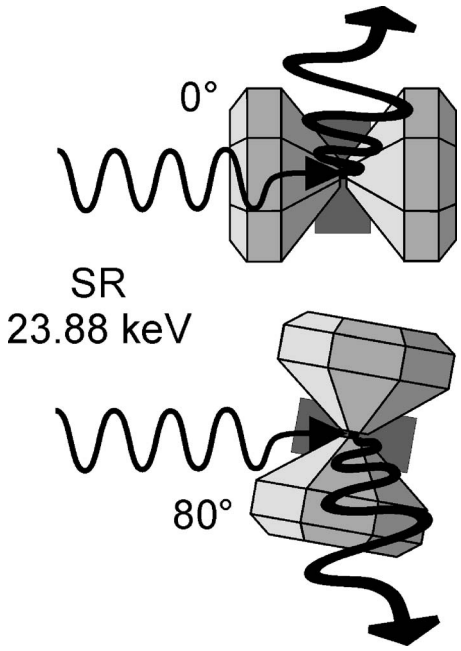

FIG. 3. Scattering geometry of the synchrotron radiation (SR). Top: sample is excited by the SR through the diamonds. The (001)-texture axis (*c* axis in Fig. 1) of the SnO powder is parallel to the beam (0° configuration). Bottom: sample is irradiated through the Be gasket. The (001)-texture axis is almost perpendicular to the beam (80° configuration).

perpendicular (80° geometry) to load axis of the cell[23] (see Fig. 3). Pressure was measured by the ruby luminescence method.[28] We used nitrogen as pressure-transmitting medium to avoid the orthorhombic distortion of the lattice due to possible nonhydrostatic pressure conditions in the sample volume.[3,12] The sample was loaded into a Be-gasket, which allowed a full transmission of the ^{119}Sn-Mössbauer γ-rays with an energy E_0 of 23.880 keV. NRIXS spectra were recorded at ambient pressure, 1.3 GPa, and 6.1 GPa in the 0° and 80° geometry. At 8.0 GPa, one spectrum was recorded in the 80° geometry.

The ambient pressure NRIXS experiments were performed with the SnO powder embedded and pressed in paraffin in order to increase and to fix the preferred orientation of the SnO crystallites. The (001)-texture is perpendicular to the pressed paraffin plane. This SnO absorber was placed in the SR beam with the texture axis parallel and almost perpendicular to the beam like the high-pressure cell.

The NRIXS experiments were performed at the undulator beamline (3ID) of the Advanced Photon Source (APS) with a high-resolution (0.83 meV) monochromator employing two pairs of Si[4 4 4] and Si[12 12 12] crystals.[29] An energy range of ±70 meV was scanned in steps of 0.2 meV. The x-ray beam was focused by two Pt-coated Kirkpatrick-Baez mirrors to a 10 μm×20 μm area impinging on the ^{119}SnO sample in the DAC. The inelastic resonant excitations were observed by collecting the delayed ^{119}Sn γ-quanta with two avalanche photodiode detectors (APD) placed perpendicular to the beam.[21,23] Typically, 8 and 16 NRIXS spectra, each collected in 1 h, were measured with a parallel (0°) and almost perpendicular (80°) orientation of the DAC with respect to the beam, then summed and converted to the phonon DOS spectra.[20]

The calculation of the partial Sn phonon DOS as a function of pressure is carried out in the framework of the shell model derived in Ref. 17. This model is based on potential short-range interactions of the Buckingham form between pairs of ions as well as long-range Coulomb interactions among all ions (see Ref. 17 for further details). The effect of pressure in the calculations is taken into account by the corresponding change in the structural parameters a, c, and z as observed experimentally.[3,12]

The fact that the model is based on potential short-range interactions among ions allows us to derive directly the force constants between neighboring ions as their distances change as function of the external pressure.

III. RESULTS AND DISCUSSION

A. Experimental and theoretical Sn DOS of SnO

^{119}Sn-NRIXS spectra measured in 0° and 80° orientation of the absorber for ambient pressure, 1.3 GPa, and 6.1 GPa are shown in Fig. 4. Due to the low Lamb-Mössbauer factor f_{LM} of 0.28 at ambient pressure, half of the inelastic scattered intensity is due to multiphonon scattering as shown in Fig. 4(a). The better statistical accuracy in the ambient pressure spectra is due to the higher count rate, which evolves from the better scattering conditions of the sample outside of the DAC. Significant differences in the 0° and 80° NRIXS spectra at ambient pressure are clearly visible.

The Sn phonon DOS, $g(E)$, of SnO at various pressures, derived from the measured NRIXS spectra by subtraction of multiphonon excitations and by the elastic line,[20] are shown in Fig. 5. The strong differences in the DOS spectra at ambient pressure for the two different directions become smaller under pressure and nearly vanish at 6.1 GPa.

The shell-model calculations of the phonon dispersions along the main symmetry directions for $p=0$ and $p=1.3$ GPa are shown in Fig. 6. Due to the improvement of this model with respect to that used in Ref. 16 to account for the specific heat as a function of temperature,[17] the dispersion curves at ambient pressure in Fig. 6 show some differences compared to the corresponding previous result (see Fig. 1 in Ref. 16), although the qualitative behavior is similar.

A gap arising between the A_{1g} and A_{2u} optical phonons around 26 and 30 meV, respectively, in the dispersion curves at ambient pressure (see Fig. 6 and Fig. 7) separates the low-energy phonons involving mainly Sn displacements from the high-energy phonons with main contributions of the oxygen atoms. Actually, we will see below that the calculated partial Sn phonon DOS extends to approximately 26 meV [see Fig. 8(a)]. This gap between the optical Sn and O modes is also visualized in the plot of the partial Sn and O DOS shown in Fig. 3 of Ref. 16.

Notice the large longitudinal-transversal (LO-TO) energy splittings of about 20 meV arising in the calculation for the infrared optical phonons A_{2u} and E_u (see the corresponding phonon labels in the M-Γ-Z direction in Fig. 6). These

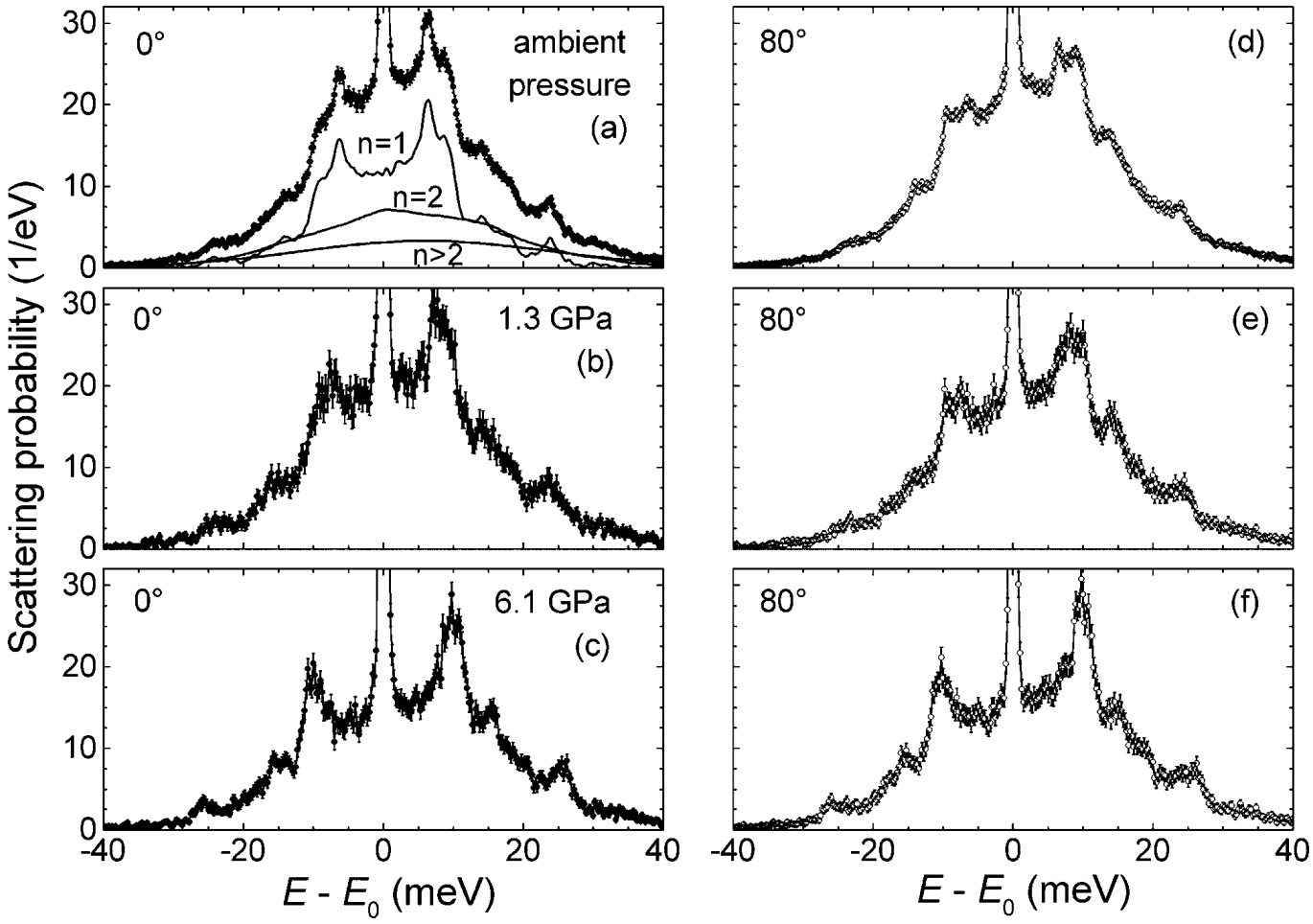

FIG. 4. ^{119}Sn-NRIXS spectra of SnO at various pressures and orientations, measured in (a)–(c) in the 0° geometry and in (d)–(f) in the 80° geometry. In spectrum (a), the one-phonon, two-phonon, and n-phonon ($n>2$) contributions are indicated.

LO-TO splittings of the infrared modes, which are due to the presence of the macroscopic electric field at long wavelengths, were also found to be quite large in a recent shell-model calculation for the metal hydride MgH_2.[30]

As the pressure increases, we observe, as expected, a general tendency to an increase in the calculated phonon frequencies of the different branches (see Fig. 6). This is reflected in a positive value for the Grüneisen parameters as will be discussed below. An exception to this behavior is found for the A_{2u}^{TO} mode and the lowest phonon modes at $M=(0.5,0.5,0)$ and $R=(0.5,0,0.5)$, which seemingly soften with pressure in the calculation. The frequency of the M-mode becomes zero around 2.9 GPa, while that of the R-mode vanishes around 2.5 GPa (see Fig. 6), which defines the limit for the application of the present shell model.

The comparison between the experimental curves and the shell-model calculations for the partial Sn phonon DOS at $p=0$ and 1.3 GPa is shown in Fig. 8. In order to account for the real polycrystalline case (no texture), the experimental curves are in a first approximation a combination of the 0° and 80° spectra in the ratio 1:2. The calculated DOS spectra show rather good agreement with the experimental DOS in their principal features. There is, however, a general small shift to lower energies for the theoretical DOS, best visualized by the dominant three bands with maximal intensities around 10, 14, and 24 meV, and a pronounced pseudogap around 20 meV. This shift is more pronounced for the maximum of the low-energy band. These main three bands are related with phonon branches ending at the lowest frequency mode at the M and R points, or converging to the $E_g^{(1)}$ and the A_{1g} phonons, respectively. The deviations between theoretical and experimental DOS at $p=1.3$ GPa are even smaller, except at low energies. The experimental peak intensities are also quite well reproduced by the calculations with the exception of the peak intensity for the 24 meV band, which is narrower than the experimental one. Here, the energy resolution of 0.83 meV of the monochromator, which is not convoluted to the theoretical data, may explain in part this difference in width.

The observed differences in energy, especially at low energies, indicate that we are, presumably due to the complex behavior of the Sn lone electron pair,[15] probably underestimating the interlayer Sn-Sn interactions. This results, for instance, in a flat dispersion branch in the Γ-Z direction related to the A_{1g} mode (see Fig. 6) leading to a narrower 24 meV band as observed in Fig. 8, and, as discussed later in detail, in the artificial softening of some low-energy modes.

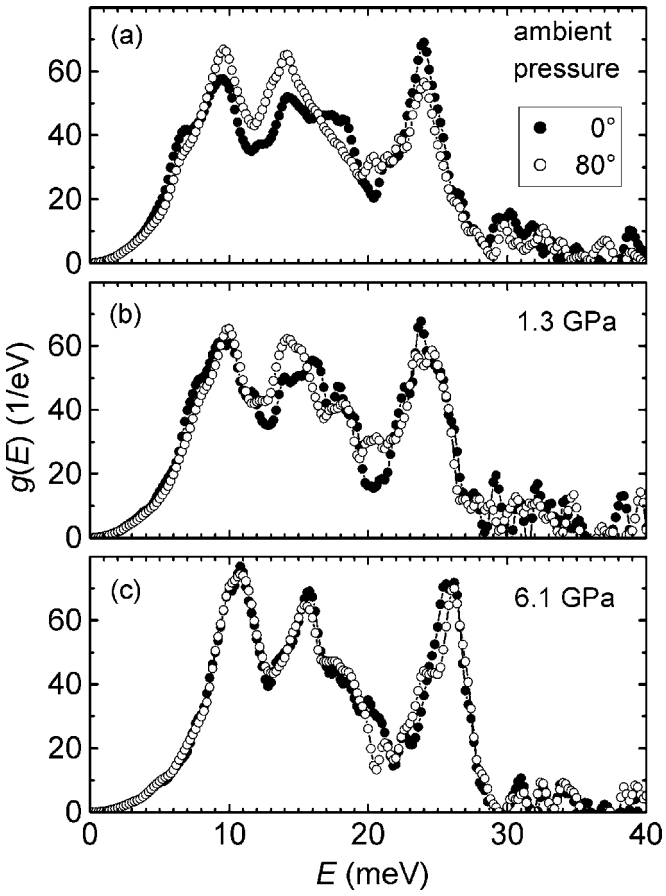

FIG. 5. Partial Sn phonon DOS in SnO with increasing pressure. The spectra were measured with textured SnO absorbers (a) in pressed paraffin or (b) and (c) in the high-pressure cell.

B. Thermodynamic and elastic properties of the Sn sublattice in SnO

The Lamb-Mössbauer factor f_{LM}, the mean force constant D, the high-temperature Debye temperature $\Theta_{\mathrm{D,HT}}$, the vibrational contributions to the Helmholtz free energy F_{vib}, to the specific heat c_{V}, to the entropy S_{vib}, and to the internal energy U_{vib} for the Sn sublattice in SnO are calculated from the integration of the corresponding experimental and theoretical partial phonon DOS $g(E)$ (cf. Figs. 5 and 8) according to the following formulas:[20,31]

$$f_{\mathrm{LM}} = \exp\left[-E_{\mathrm{R}}\int_0^\infty \frac{g(E)}{E}\coth(x)dE\right], \tag{1}$$

$$D = \frac{M}{\hbar^2}\int_0^\infty g(E)E^2dE, \tag{2}$$

$$\Theta_{\mathrm{D,HT}} = \frac{4}{3k_{\mathrm{B}}}\int_0^\infty g(E)EdE, \tag{3}$$

$$F_{\mathrm{vib}} = 3k_{\mathrm{B}}T\int_0^\infty g(E)\ln[2\sinh(x)]dE, \tag{4}$$

$$c_{\mathrm{V}} = \left(\frac{\partial U}{\partial T}\right)_{\mathrm{V}} = 3k_{\mathrm{B}}\int_0^\infty g(E)x^2\sinh^{-2}(x)dE, \tag{5}$$

$$S_{\mathrm{vib}} = -\left(\frac{\partial F}{\partial T}\right)_{\mathrm{V}} = 3k_{\mathrm{B}}\int_0^\infty g(E)\{x\coth(x) - \ln[2\sinh(x)]\}dE, \tag{6}$$

$$U_{\mathrm{vib}} = F - T\left(\frac{\partial F}{\partial T}\right)_{\mathrm{V}} = \frac{3}{2}\int_0^\infty g(E)E\coth(x)dE, \tag{7}$$

with $x=E/(2k_{\mathrm{B}}T)$, E_R=2.575 meV the recoil energy of the ^{119}Sn nucleus, $M=1.974\times10^{-25}$ kg the mass of the ^{119}Sn nucleus, and k_{B} the Boltzmann constant.

According to Sturhahn *et al.*,[19,32] the measurements of nuclear resonant inelastic scattering provide in general more reliable values of the Lamb-Mössbauer factor f_{LM} than conventional Mössbauer spectroscopy. This is because quite often the recoil-free fraction and linewidth of the radioactive source as well as the sample thickness are not considered in the spectral analysis. This may explain the wide variation of f_{LM} values in earlier Mössbauer studies of SnO at room temperature, ranging from 0.12(1) (Ref. 11) and 0.14(3) (Ref. 33) to 0.35(2) (Ref. 10) at ambient conditions compared to f_{LM}=0.28(1) from the present study. With increasing pressure, the value of f_{LM} increases to 0.40(2) at 8.0 GPa.

Since the layered litharge structure of tetragonal SnO is highly anisotropic and since the axial compressibilities of the c axis and a,b axes are differing by a factor of 7, reflecting the soft van der Waals-type interactions between the Sn-O-Sn layers, one expects also for the Sn atoms an anisotropy in the local vibrational modes, which might be reflected in an anisotropic Lamb-Mössbauer factor f_{LM} (see Ref. 10). The relationship between crystal symmetry and a phonon DOS anisotropy has been treated in general by Sturhahn and Kohn.[34] Differences in the local phonon DOS at the Sn atoms are already visible in the experimental NRIXS-spectra of SnO measured in the 0° and 80° geometry (Fig. 4) as well as in the derived phonon DOS (Fig. 5); these differences are much more pronounced in the projected phonon DOS as seen parallel and perpendicular to the c axis (see Fig. 11 in Sec. III C). Surprisingly there are, however, only small differences in the f_{LM} factor derived from the 0° and 80° spectra at ambient pressure and at 1.3 GPa in the way that the one in the 80° direction (within the a,b plane) is slightly larger, but the difference is within the error bars of the values. This means that the differences in the projected Sn phonon DOS are averaged for the derived f_{LM} values due to the integration over the whole phonon DOS [see Eq. (1)]. This behavior can be also attributed to the strong covalent bonds of the Sn atoms with four oxygen neighbors within the Sn-O-Sn layer directing neither parallel nor perpendicular to the c axis (angle between O-Sn bond and c axis is 58.9° and gets smaller at higher pressure, approaching 58.3° at 6.1 GPa). The rather isotropic behavior of the Lamb-Mössbauer factor is reflected by the absence of a significant

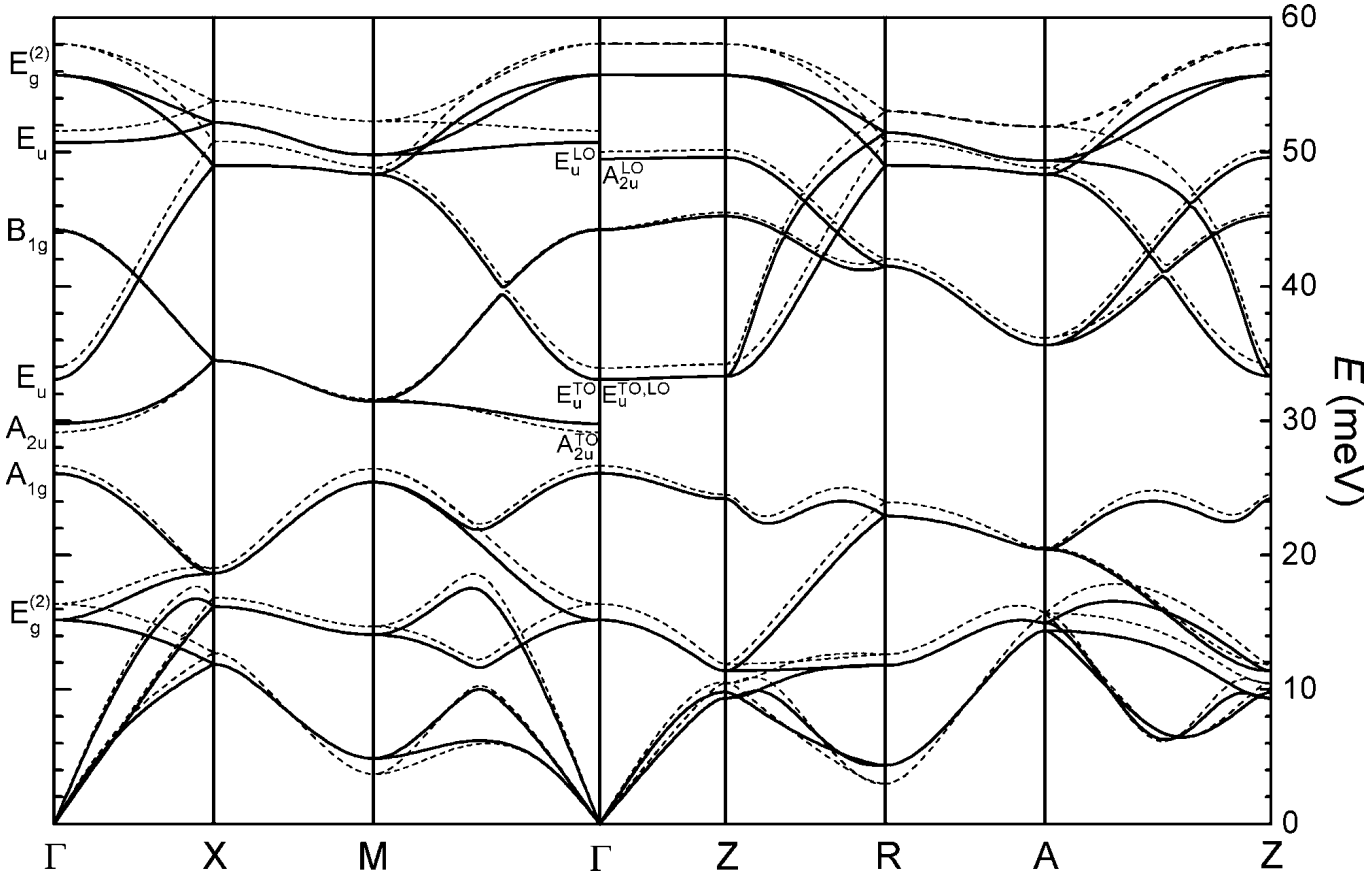

FIG. 6. Dispersion curves of SnO along the main symmetry directions of the Brillouin zone (cf. Fig. 7) calculated with the shell model of Ref. 17 at ambient pressure (solid line), and $p=1.3$ GPa (dashed lines).

Goldanskii-Karyagin effect in the quadrupole spectra of SnO in previous ^{119}Sn-Mössbauer studies by Herber[10] and Moreno.[11]

The mean force constant D is within the error bars the same for the two different geometries. This behavior can again be explained by the strong binding between the oxygen and the Sn ions. The comparison between experiment and theory of the different thermodynamic properties as a function of pressure in Fig. 9, enables us to further test the shell model developed in Ref. 17. The calculated values at ambient pressure remarkably agree within error bars with the corresponding experimental data, with the only exception of the value for F_{vib}, which deviates by about 8% from the experimental value. Moreover, the variations with pressure of the calculated values, i.e., the slope of the theoretical curves in Fig. 9, are also in good general agreement with those for the experiment. The only exception is the variation of f_{LM} with pressure, which shows an increasingly negative slope for $p>0.5$ GPa compared to the positive and pronounced increase of f_{LM} observed experimentally. The origin of this discrepancy is the above-mentioned softening with pressure of the low-energy modes around the M and R points in the shell model.

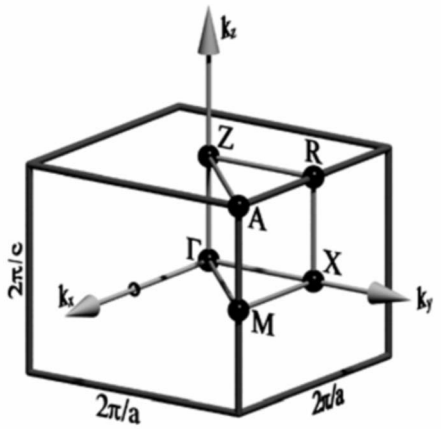

FIG. 7. First Brillouin zone of the simple tetragonal lattice of SnO. Symmetry points are indicated (to be compared with the dispersion curves in Fig. 6).

In Fig. 10 the two experimental (solid and open symbols) and theoretical (crossed symbols) Debye temperatures $\Theta_{D,HT}$ (circles) and $\Theta_{D,LT}$ (squares) are plotted, where HT denotes the so called high-temperature case obtained for $T\rightarrow\infty$, and LT the low-temperature case corresponding to the limit $T\rightarrow 0$. According to Eq. (3), $\Theta_{D,HT}$ is derived from the first moment of the whole partial phonon DOS, which leads to a Debye temperature characteristic for the Sn sublattice because the oxygen phonon DOS is not monitored by ^{119}Sn-NRIXS. On the other hand, $\Theta_{D,LT}$ is derived from the low-energy part of the experimental phonon DOS, where the Debye approximation $g(E)\propto E^2$ is valid. In this low-energy range, up to about 6 meV for SnO at ambient pressure, one

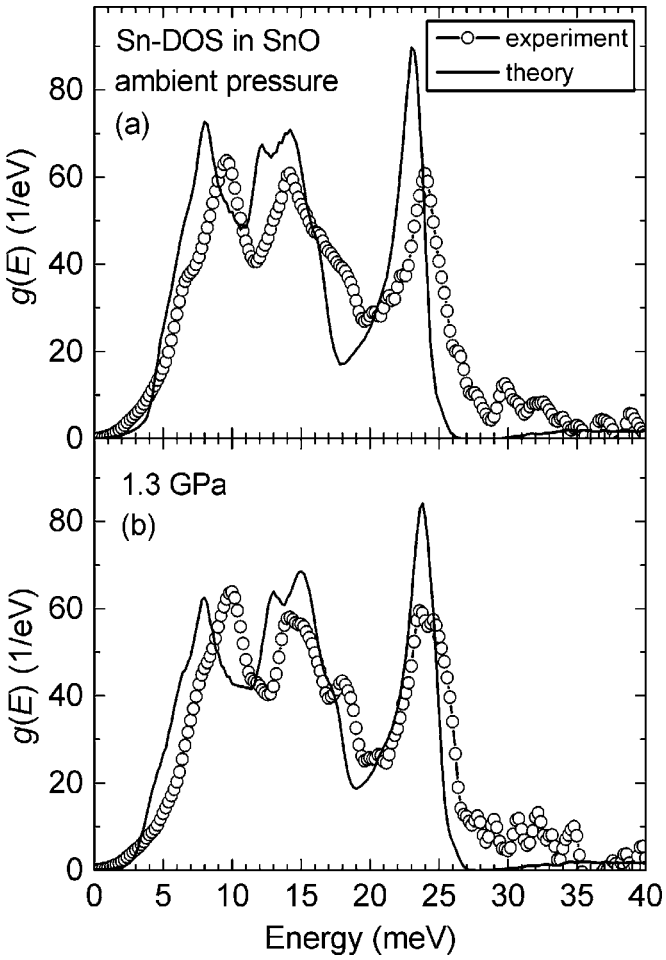

FIG. 8. Comparison between the experimental (open circles) and theoretical (solid line) partial phonon DOS of the Sn sublattice in SnO, for an ideal polycrystalline absorber without texture (see text).

actually derives the Debye sound velocity, characteristic for the whole SnO lattice, which is proportional to $\Theta_{D,LT}$ (see a recent study to this subject involving the ^{119}Sn resonance in Ref. 35). The theoretical effective Debye temperature $\Theta_D(T)$ for the Sn sublattice is obtained numerically for each T by solving the equation $c_V^D(T/\Theta_D)=c_V^{SM}(T)$, where c_V^D is the integral expression for the specific heat in the Debye approximation (see Ref. 31, p. 135) and c_V^{SM} is the shell-model specific heat obtained after integration of the theoretical Sn-DOS according to Eq. (5).[17,30] The theoretical values of $\Theta_{D,HT}$ and $\Theta_{D,LT}$ are derived from $\Theta_D(T)$ after performing the corresponding high- and low-temperature limits, respectively.

Inspection of Fig. 10 shows reasonable agreement between the theoretical and experimental $\Theta_{D,HT}$ values, which are representing the whole Sn phonon DOS. On the other hand, the theoretical values for $\Theta_{D,LT}$ in Fig. 10 are larger than the experimental ones, although the slope of the curve for $p<2$ GPa fairly agrees with the experiment. The larger values for the theory are due to the fact that the parabolic dependence of the Sn-DOS at very low energy ($\leq$4 meV) is less pronounced in the theoretical spectrum, as can be seen in Fig. 8. This indicates a probable overestimation of the elastic constants, i.e., the slope of the acoustic dispersion curves as the wave vector tends to zero, in the present shell model. The sudden drop of the theoretical curve of $\Theta_{D,LT}$ for pressures larger than 2 GPa can be related to the artificial softening with pressure of the low-energy branch related to point R of the Brillouin zone, which precludes the application of the present model as already mentioned. Actually, this softening produces a rapid increase of the Sn-DOS at low energies, which in turn affects completely the value of $\Theta_{D,LT}$ as well as alter that of the Mössbauer factor f_{LM} which has also a negative slope in its variation with increasing pressure [see Fig. 9(a)].

Also, the experimentally obtained $\Theta_{D,LT}$ and $\Theta_{D,HT}$ values exhibit an unusual behavior in that the $\Theta_{D,LT}$ value is considerably lower than the $\Theta_{D,HT}$ value. In simple monoatomic solids such as fcc and bcc metals, one observes in general larger values for $\Theta_{D,LT}$ than for $\Theta_{D,HT}$ (see, for instance, Ref. 36). This normal behavior is not observed in the analysis of the experimental partial Sn phonon DOS and can be attributed to the anomalous soft bonding between the Sn-O-Sn layers, reflected by the large difference in their axial compressibilities.[3,12] With increasing pressure, when the elastic properties and the phonon DOS become more isotropic, the $\Theta_{D,LT}$ and $\Theta_{D,HT}$ values approach and become equal at about 8 GPa (see Fig. 10). At even higher pressures, a change to a normal situation of a larger $\Theta_{D,LT}$ value is expected.

All these properties of elastic and thermodynamic parameters of SnO derived from the measured Sn DOS are listed in Table I and will be discussed below in view of their directional dependencies in the following Sec. III C.

C. Projected phonon DOS, phonon-mode analysis, and Grüneisen parameters

As mentioned in the Introduction, it is possible to extract by the subtraction method from the phonon DOS of textured samples, which is measured in different directions with respect to the texture axis, the phonon DOS as seen parallel and perpendicular to the texture axis (here the tetragonal c axis of SnO). The principles were first outlined in Ref. 34 and experimentally first applied to the phonon DOS of hcp Fe.[23,24] Since the resonant scattering probability of the incident x-rays with respect to the local phonon DOS is a second-rank tensor, it follows for the tetragonal lattice of SnO that the ^{119}Sn-NRIXS spectra are measured with a $\cos^2\phi$ dependence with respect to the partial phonon DOS shown in Fig. 5, where ϕ is the angle (in r space) between the polarization vector of the phonon mode with respect to the k vector of the incident x-ray. In case of a single-crystalline SnO sample, one would observe with the x-rays parallel to the c axis the Γ-Z modes of the Brillouin-zone (see Fig. 7) with full intensity, the modes in the Γ-A and Γ-R directions contribute with their $\cos^2\phi$ intensity, whereas the modes perpendicular to the c axis, Γ-X and Γ-M are not observed. With the x-rays perpendicular to the c axis, these latter modes would fully contribute, the Γ-R and Γ-A modes according to their $\cos^2\phi'$ intensity ($\phi'=90°-\phi$), whereas

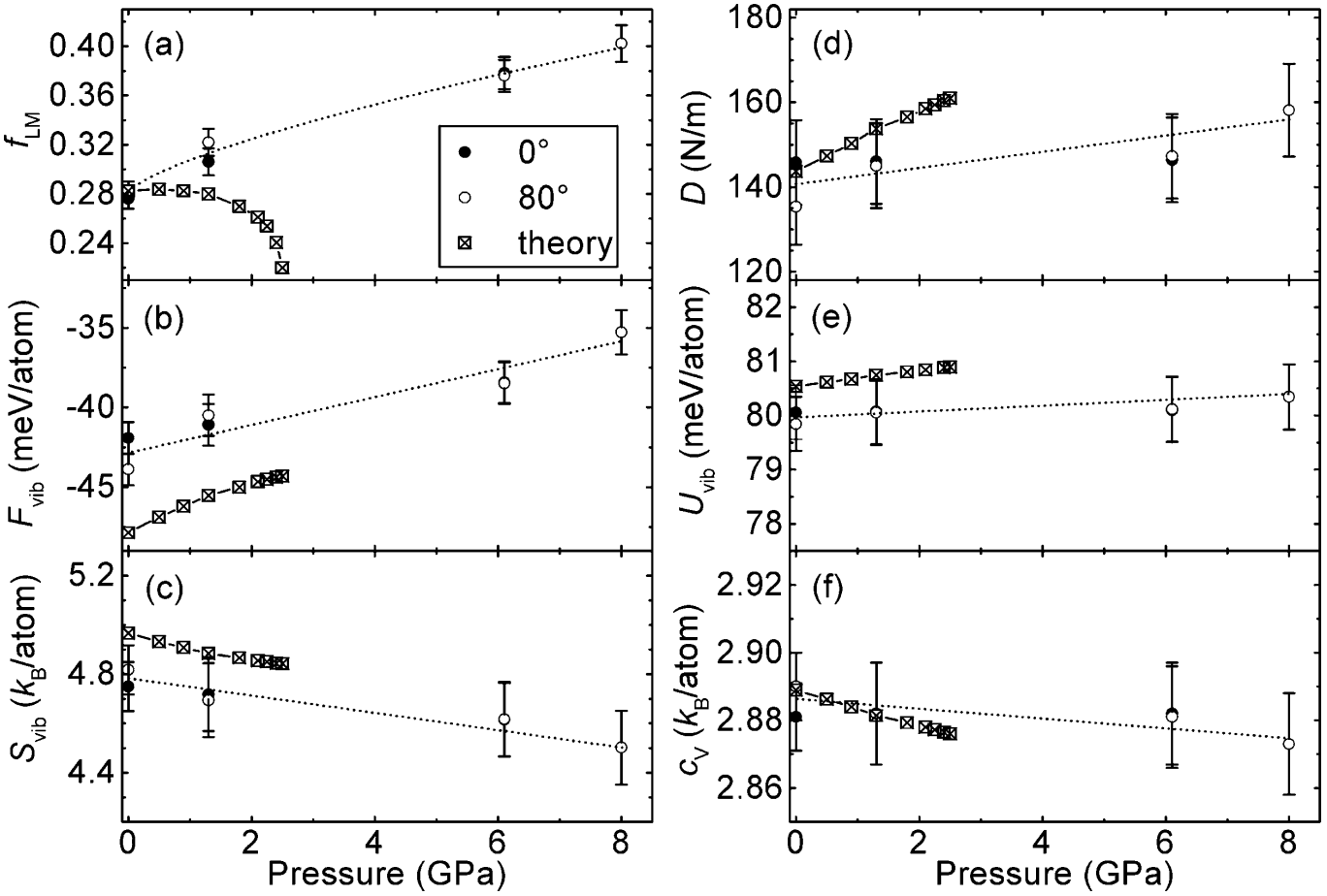

FIG. 9. Pressure dependence of the thermodynamic and elastic parameters of the Sn sublattice in SnO. Solid dots are from measurements in the 0° geometry and open dots in the 80° geometry. The dotted lines are guides to the eye. The crossed squares are the theoretical results obtained in the present work using the shell model developed in Ref. 17.

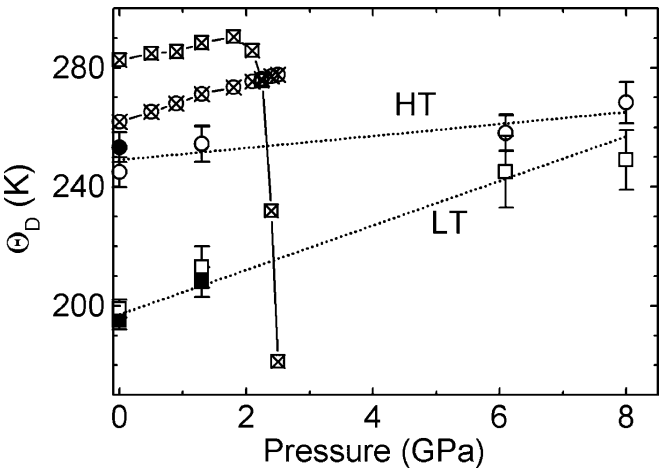

FIG. 10. The high-temperature (HT) (circles) and low-temperature (LT) (squares) Debye temperatures $\Theta_{D,HT}$ and $\Theta_{D,LT}$ of the Sn sublattice in SnO. Solid (open) symbols are from the 0° (80°) geometry. The crossed circles and crossed squares are the corresponding theoretical values for $\Theta_{D,HT}$ and $\Theta_{D,LT}$, respectively, obtained with the shell model of Ref. 17.

the Γ-Z mode is not detectable. All other modes between these principle directions would contribute accordingly to their $\cos^2 \phi'$ dependence.

The derivation of the projected Sn phonon DOS as seen by a single crystalline SnO sample parallel and perpendicular to the c axis from the measured phonon DOS depends critically on the degree of texture of the investigated sample. As outlined in the Appendix and applied already for the case of hcp Fe,[23,24,37] the subtraction of measured phonon DOS spectra with different directions with respect to the texture axis can enforce the degree of texture approaching the case of a single-crystalline sample. For this purpose, we subtracted from the phonon DOS derived from NRIXS spectra at ambient pressure in the 0° direction the phonon DOS obtained for the 80° direction, the latter weighted with factors $\zeta_{0°}$ ranging from 0.1 to 0.9 and renormalized these difference spectra. For $\zeta_{0°}=0.7$ we obtained a phonon DOS with no negative contributions (which are, of course, physically not possible), indicating the right choice of the $\zeta_{0°}$ parameter. From this value of $\zeta_{0°}$ one can derive the degree of texture, $w=0.17$, and also the corresponding subtracting factor $\zeta_{80°}=0.43$ for the phonon DOS measured at 80°. A correspond-

TABLE I. Elastic and thermodynamic parameters of the Sn sublattice derived from the experimental partial Sn phonon DOS of SnO.

SnO	p (GPa)	f_{LM}	$\Theta_{D,HT}$ (K)	$\Theta_{D,LT}$ (K)	D (N/m)	F_{vib} (meV/atom)	U_{vib} (meV/atom)	c_V (k_B/atom)	S_{vib} (k_B/atom)
0°	0	0.276(8)	253(5)	195(3)	146(10)	−41.9(10)	80.1(5)	2.881(10)	4.75(10)
0°	1.3	0.306(11)	254(6)	208(5)	146(10)	−41.1(13)	80.1(6)	2.882(15)	4.72(15)
0°	6.1	0.378(13)	258(6)	245(12)	146(11)	−38.4(13)	80.1(6)	2.882(15)	4.62(15)
80°	0	0.283(7)	245(5)	199(3)	135(9)	−43.9(10)	79.8(5)	2.890(10)	4.82(10)
80°	1.3	0.322(11)	255(6)	213(7)	145(10)	−40.5(13)	80.1(6)	2.882(15)	4.69(15)
80°	6.1	0.376(13)	258(6)	245(12)	147(10)	−38.5(13)	80.1(6)	2.881(15)	4.62(15)
80°	8	0.402(15)	268(7)	249(10)	158(11)	−35.3(14)	80.3(6)	2.873(15)	4.50(15)
proj. 0°	0	0.25(2)	274(8)	189(5)	171(15)	−37.2(16)	80.6(10)	2.864(17)	4.59(18)
proj. 90°	0	0.28(2)	238(8)	197(5)	127(14)	−45.5(16)	79.7(10)	2.898(17)	4.88(18)

ing treatment of the phonon DOS spectra measured in the 0° and 80° direction in the high-pressure cell shows that the preferred orientation is larger with a degree of texture of $w=0.24$, with the subtraction factors $\zeta_{0°}=0.6$ and $\zeta_{80°}=0.32$, respectively.

The derived experimental projected phonon DOS in the 0° and 90° directions with respect to the c axis of SnO are shown in Fig. 11 together with the theoretical projected phonon DOS. The theoretical phonon DOS projected along the α direction is determined by the following expression:

$$g_{\alpha\kappa}(\omega) = \int_{BZ_i} W(\vec{q}) d^3\vec{q} \sum_j e_{\alpha\kappa}(\vec{q}j) e^*_{\alpha\kappa}(\vec{q}j) \delta[\omega - \omega_j(\vec{q})], \tag{8}$$

where α is a Cartesian coordinate index, κ is atom index, $e_{\alpha\kappa}(\mathbf{q},j)$ is the α component of the eigenvector for atom κ, j is the branch index, and ω are phonon frequencies. The integration is made over the irreducible Brillouin zone (BZ_i), and $W(\mathbf{q})$ are the corresponding weight factors for each point $\mathbf{q}$ in the irreducible zone.

Both the projected experimental and theoretical phonon DOS can be used to analyze and discuss the properties of the phonon modes directed parallel and perpendicular to the c axis, especially the optical modes A_{1g} and $E_g^{(1)}$ at Γ, the center of the Brillouin zone, accessible by Raman spectroscopy (see Fig. 6).

The projected Sn phonon DOS spectra in the direction parallel to the c axis (left panel of Fig. 11) exhibit now, due to the enhanced selectivity by the subtraction method, better resolved structures, which allows a much better identification and comparison between experimental and theoretical data as in the polycrystalline case (see Fig. 8). Two of these structures, clearly resolved in the projected DOS at ambient pressure around 8–10 meV and 24 meV, are marked with $P1$ and $P2$, respectively. In the experimental DOS, they both shift to higher energies with increasing pressure. This shift is much more pronounced for structure $P1$, which also narrows with pressure. Theoretically, the structure $P1$, which can be mainly attributed to transversal and longitudinal acoustic branches approaching the Z point in the Brillouin zone (see Fig. 6), has a pressure behavior contrary to the experiment, i.e., it shifts to lower energies as pressure increases. This trend is produced by the lowering of the lowest R and M modes and related branches with pressure in the theoretical

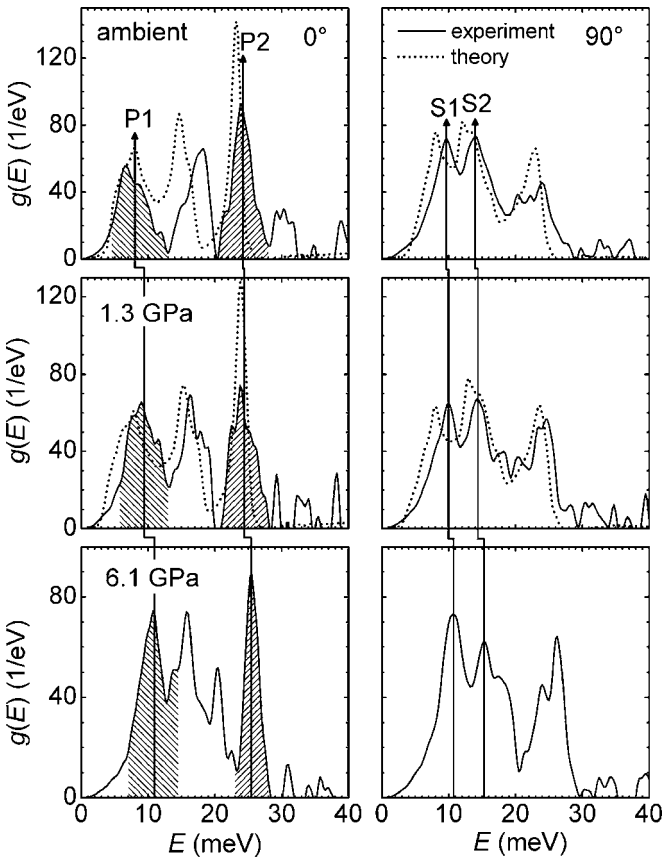

FIG. 11. The experimental subtracted partial phonon DOS (solid lines) of the Sn site in SnO. The left column shows the projected DOS along the c axis and the right column those in the a,b plane (see Fig. 1). The vertical lines denote the positions of characteristic features indicated as $P1$, $P2$, $S1$, and $S2$. The dotted lines represent the theoretical projected partial phonon DOS over (left column) the c direction and (right column) the a,b plane, obtained with the shell model derived in Ref. 17.

TABLE II. Zone-center phonon energies of the modes $E_g^{(2)}$, A_{1g}, and $E_g^{(1)}$ (see Fig. 6) at ambient pressure and their Grüneisen parameters. The data for the A_{1g} and $E_g^{(1)}$ Raman modes (Ref. 12) are compared with theoretical calculations from Ref. 15 and our present shell model as well as with our NRIXS results of the modes labeled $P2$ and $S2$ in Fig. 11.

Mode	Raman Ref. 12	FP-LAPW Ref. 15	Shell-model this work	Sn-NRIXS this work
$E_g^{(2)}$		56.4 meV	55.8 meV	
		(455 cm^{-1})	(450 cm^{-1})	
		0.6	0.59	
A_{1g}	26.2 meV	25.8 meV	26.2 meV	
	(211 cm^{-1})	(208 cm^{-1})	(211 cm^{-1})	
	0.38(4)	0.3	0.27	0.5(1) (P2)
$E_g^{(1)}$	14.0 meV	14.0 meV	15.1 meV	
	(113 cm^{-1})	(113 cm^{-1})	(122 cm^{-1})	
	0.80(8)	0.8	1.79	0.8(1) (S2)

dispersion relations, which also leads to an increase of the DOS intensity around 5 meV in the 1.3 GPa DOS, visible already in the polycrystalline data (see Fig. 8). On the other hand, the narrow structure and pressure-induced shift of $P2$ at 24 meV agree well in both theoretical and experimental data and will be discussed below with the related A_{1g} Raman mode.

The projected experimental and theoretical DOS spectra perpendicular to the c axis exhibit three spectral features, but only the two at lower energies, marked $S1$ and $S2$, are undoubtedly retraceable in both experimental and theoretical data. The comparison of the theoretical and experimental spectra enables again an identification of the optical modes detectable with the Raman effect. Here we attribute the $S2$ structure at 14 meV in the experimental DOS to the a,b-polarized $E_g^{(1)}$ mode. The $S1$ structure can be related to acoustic phonon branches in different symmetry directions (see Fig. 6).

The experimentally observed pressure dependence of the $P2$ and $S2$ band maxima can be related to the pressure dependence of the corresponding Γ-point modes due to the fact that in the Debye-Grüneisen model the pressure-induced frequency shifts of the related phonon branches are proportional to their energy and can be expressed by the corresponding mode-Grüneisen parameter

$$\gamma_i = -\frac{d \ln \omega_i}{d \ln V}. \tag{9}$$

Thus, the volume dependence of the frequency ω_i of the maxima $P2$ and $S2$ can be derived from the pressure dependence of the $P2$ and $S2$ modes using the measured pV relations of the SnO lattice[3,12] and compared with the Grüneisen parameters of the A_{1g} and $E_g^{(1)}$ modes, respectively, obtained from Raman studies.[12] The experimental γ_i values for the $P2$ and $S2$ modes as well as of the A_{1g} and $E_g^{(1)}$ modes are compiled in Table II. The Grüneisen parameters of the A_{1g}, $E_g^{(1)}$, and $E_g^{(2)}$ zone-center modes calculated by the present theoretical shell model are also listed in Table II together with the values from other theoretical calculations.[15] Although the γ_i values were not explicitly determined in Ref. 15, we have computed them from the following formula:

$$\gamma_i = \left(\frac{1}{\omega_i}\right)\left(\frac{\Delta\omega_i}{\Delta p}\right)B_0, \tag{10}$$

where the values of $(\Delta\omega_i/\Delta p)$ were approximately obtained by a linear regression of the data in Figs. 8 and 9 of Ref. 15, and we considered $B_0=38$ GPa for the bulk modulus as was experimentally obtained in Ref. 12.

Considering the assumptions made above within the Debye-Grüneisen approximation by comparing the Raman modes with the maxima of the corresponding modes in the projected phonon DOS, there is very good agreement between the Raman and the Sn-NRIXS data, especially for the $E_g^{(1)}$ mode. As pointed already out in Ref. 17, the present shell model can excellently reproduce the frequencies of the A_{1g} Raman mode at ambient pressure and fairly well its pressure dependence (see Table II). The energy and pressure dependence of the $E_g^{(2)}$ mode obtained with the present shell model are found in remarkably agreement with the *ab initio* data of Ref. 15. The $E_g^{(1)}$ Raman mode, now unambiguously observed at 14.0 meV (113 cm^{-1}),[12] is calculated in the shell model at 15.1 meV (122 cm^{-1}), its calculated Grüneisen parameter is twice as large as the Raman and NRIXS values; the latter values, on the other hand, agree well with a LAPW calculation.[15] As already shown in Ref. 17 and discussed in Ref. 15, the LAPW method is more appropriate for the *ab initio* determination of this low-energy Raman mode.

The experimental and most theoretical γ_i values in Table II for optical modes are smaller than 1, especially the ones for the A_{1g} mode. These are unusual small values when compared with γ_i values of regular solids ranging between 1 and 2. This may be explained by the fact that these modes are mainly intralayer modes not as much influenced by the change in volume as interlayer modes. The latter are much more susceptible to the reduction of volume, which causes, due to the highly anisotropic compression of the c axis and a,b axes, combined with the change in the Sn position parameter z, a strong change of the Sn-Sn interlayer distance. The acoustic modes contained in the structure $P1$ (see Fig. 11) reflect this drastic change of the structural parameters in the c direction by values of $\gamma_{P1}=4.4$ between 0 and 1.3 GPa and $\gamma_{P1}=1.9$ for 1.3 to 6.1 GPa. Due to the artificial softening with pressure of the acoustic modes at M and R and related branches in the Brillouin zone, the present shell model derives unphysical negative γ_i values for them. In future applications of the shell model, the interaction parameters may be modeled in a way to meet the experimental trend with pressure in the low-energy region.

IV. SUMMARY

We have measured the partial phonon DOS of the Sn sublattice in SnO up to 8 GPa applying the new method of ^{119}Sn-NRIXS. The preferred orientation of the SnO crystallites was used to measure the partial phonon DOS parallel

and almost perpendicular to the texture axis of the SnO samples. Applying a recently developed subtraction method, we derived from these phonon DOS of textured SnO absorbers the projected phonon DOS as seen parallel and perpendicular to the c axis of tetragonal SnO. These projected phonon DOS spectra are used for a mode-specific analysis by comparing with theoretically calculated phonon DOS. For this purpose, we computed the corresponding Sn phonon DOS as a function of pressure and orientation by means of a shell model developed recently.[17] We found good agreement between the experimentally and theoretically derived phonon DOS, especially for optical modes at higher energies, as well as good agreement with recent Raman studies of the A_{1g} and $E_g^{(1)}$ modes, including their Grüneisen parameters.[12] Different thermodynamic and elastic properties obtained by integration of the DOS spectra also show general good agreement between theory and experiment in their behavior with pressure. The present shell model, however, fails to calculate the properties of the low-energy modes, here especially the acoustic modes, as reflected in the failure to calculate the pressure dependence of the Lamb-Mössbauer factor f_{LM} and that of $\Theta_{\mathrm{D,LT}}$ at pressures larger than 2 GPa. The reasons for this are obviously the complex electronic inter- and intralayer interactions, caused by the lone electron pair of the Sn^{2+} ions, as pointed out by recent *ab initio* calculations of the electronic structure of SnO.[15]

These complex binding properties in the layered SnO structure are also reflected in the highly anisotropic compressibility,[3,12] in the projected phonon DOS spectra, and in the derived elastic and thermodynamic parameters, most pronounced in the Debye temperatures $\Theta_{\mathrm{D,HT}}$ and $\Theta_{\mathrm{D,LT}}$ of the Sn sublattice. We observe the unusual case that the experimental value of $\Theta_{\mathrm{D,LT}}$ is considerably smaller than that of $\Theta_{\mathrm{D,HT}}$. With increasing pressure, this difference is reduced, as is also the marked differences in the projected phonon DOS and derived parameters, indicating that the SnO lattice becomes more isotropic in all elastic properties at higher pressures.

ACKNOWLEDGMENTS

H.G. and G.W. thank Karl Syassen for making preprints available prior to publication. S.K. acknowledges helpful discussions with R. Migoni and thanks Fundación Antorchas, Argentina, for support. S.K. also acknowledges partial support from CONICET, Argentina. This work was supported by the U.S. Department of Energy, Office of Science, Basic Energy Sciences, under Contract No. W-31-109-Eng-38 and by the German BMBF (Grant No. 05 KS4PPB/4).

APPENDIX: SUBTRACTION METHOD

According to Refs. 38 and 39, the projected phonon DOS $g(E,\mathbf{s})$ is proportional to $|\mathbf{s}\mathbf{e}_j(\mathbf{q})|^2$, where E is the energy, $\mathbf{s}$ is the normalized wave vector of the incident γ ray $\mathbf{k}/|\mathbf{k}|$, $\mathbf{e}_j(\mathbf{q})$ is the polarization vector of vibrations in the mode $\{\mathbf{q}j\}$. The value of $|\mathbf{s}\mathbf{e}_j(\mathbf{q})|^2$ matches the value of $\cos^2\phi$. Here, ϕ is the angle between the wave vector $\mathbf{k}$ and the polarization vector $\mathbf{e}_j$ of the phonon.

To increase the differences in the measured phonon DOS, we introduce the following method which is suitable for a simple preferred orientation of a powder with a tetragonal or hexagonal unit cell (one axis of the unit cell shows a preferred orientation; the other two equal axes in that orthogonal system are perpendicular to the preferred orientation but statistically distributed in that plane).

The two measured phonon DOS $(0°,80°)$ of a textured powder, where the preferred orientation is parallel to the SR $[g_0(E)]$ and almost perpendicular $[g_{80}(E)]$, contain always a certain part of the randomly distributed powder sample. To reduce this background from the two spectra, a certain part of one spectrum is subtracted from the other one. The subtraction factor ζ $(0\leq\zeta\leq1)$ depends on the magnitude of the texture and the angle between the SR and the texture axis. The preferred orientation has a value of w $(0\leq w\leq1)$, where $w=1$ means complete simple preferred orientation and $w=0$ a pure powder sample without texture. One has to pay attention that the new DOS spectra $[g_0'(E),g_{90}'(E)]$ do not contain negative density of states. This can be influenced by the subtraction factor ζ which is different for the two directions,

$$g_0'(E)=g_0(E)-\zeta_0 g_{80}(E), \tag{11}$$

$$g_{90}'(E)=g_{80}(E)-\zeta_{80} g_0(E). \tag{12}$$

These new generated DOS spectra, which represent the projected DOS spectra along the corresponding directions, are here called subtracted DOS. The calculation of ζ_0 and ζ_{90} can be found in Ref. 37.

*Corresponding author. Email address: hubertus@physics.unlv.edu

[1] Z. Han, N. Guo, F. Li, W. Zhang, H. Zhao, and Y. Qian, Mater. Lett. **48**, 99 (2001), and references therein.
[2] H. Giefers, F. Porsch, and G. Wortmann, Phys. Scr. **T115**, 538 (2005).
[3] H. Giefers, F. Porsch, and G. Wortmann, Physica B **373**, 76 (2006).
[4] F. Izumi, J. Solid State Chem. **38**, 381 (1981).
[5] H. Giefers, F. Porsch, and G. Wortmann, Solid State Ionics **176**, 199 (2005).
[6] H. Giefers, F. Porsch, and G. Wortmann, Solid State Ionics **176**, 1327 (2005).
[7] J. D. Donaldson, W. Moser, and W. B. Simpson, J. Chem. Soc. **1961**, 839.
[8] W. Kwestroo and P. H. G. M. Vromans, J. Inorg. Nucl. Chem. **29**, 2187 (1967).
[9] V. N. Panyushkin and L. V. Rumyantseva, Sov. Phys. Crystallogr. **13**, 603 (1969).
[10] R. H. Herber, Phys. Rev. B **27**, 4013 (1983).
[11] M. S. Moreno and R. C. Mercader, Phys. Rev. B **50**, 9875 (1994).

[12] X. Wang, F. X. Zhang, I. Loa, K. Syassen, M. Hanfland, and Y.-L. Mathis, Phys. Status Solidi B **241**, 3168 (2004).
[13] N. R. Serebryanaya, S. S. Kabalkina, and L. F. Vereshchagin, Sov. Phys. Dokl. **14**, 672 (1970).
[14] D. M. Adams, A. G. Christy, J. Haines, and S. M. Clark, Phys. Rev. B **46**, 11358 (1992).
[15] N. E. Christensen, A. Svane, and E. Peltzer y Blancá, Phys. Rev. B **72**, 014109 (2005).
[16] S. Koval, M. G. Stachiotti, R. L. Migoni, M. S. Moreno, R. C. Mercader, and E. L. Peltzer y Blancá, Phys. Rev. B **54**, 7151 (1996).
[17] S. Koval, R. Burriel, M. G. Stachiotti, M. Castro, R. L. Migoni, M. S. Moreno, A. Varela, and C. O. Rodriguez, Phys. Rev. B **60**, 14496 (1999).
[18] M. Seto, Y. Yoda, S. Kikuta, X. W. Zhang, and M. Ando, Phys. Rev. Lett. **74**, 3828 (1995).
[19] W. Sturhahn, T. S. Toellner, E. E. Alp, X. Zhang, M. Ando, Y. Yoda, S. Kikuta, M. Seto, C. W. Kimball, and B. Dabrowski, Phys. Rev. Lett. **74**, 3832 (1995).
[20] W. Sturhahn, J. Phys.: Condens. Matter **16**, S497 (2004).
[21] R. Lübbers, H. F. Grünsteudel, H. F. Chumakov, and G. Wortmann, Science **287**, 1250 (2000).
[22] H. K. Mao, J. Xu, V. V. Struzhkin, J. Shu, R. J. Hemley, W. Sturhahn, M. Y. Hu, E. E. Alp, L. Vocadlo, D. Alfé, G. D. Price, M. J. Gillan, M. Schwoerer-Böhning, D. Häusermann, P. Eng, G. Shen, H. Giefers, R. Lübbers, and G. Wortmann, Science **292**, 914 (2001).
[23] H. Giefers, R. Lübbers, K. Rupprecht, G. Wortmann, D. Alfé, and A. I. Chumakov, High Press. Res. **22**, 501 (2002).
[24] H. Giefers, G. Wortmann, A. I. Chumakov, and D. Alfé, *ESRF Highlights*, edited by G. Admans (ESRF, Grenoble, 2004), p. 18.
[25] A. I. Chumakov, A. Barla, R. Rüffer, J. Metge, H. F. Grünsteudel, H. Grünsteudel, J. Plessel, H. Winkelmann, and M. M. Abd-Elmeguid, Phys. Rev. B **58**, 254 (1998).
[26] M. Y. Hu, Ph.D. thesis, Northwestern University, 1999.
[27] E. E. Alp, T. M. Mooney, T. Toellner, W. Sturhahn, E. Witthoff, R. Röhlsberger, E. Gerdau, H. Homma, and M. Kentjana, Phys. Rev. Lett. **70**, 3351 (1993).
[28] H. K. Mao, P. M. Bell, J. W. Shaner, and D. J. Steinberg, J. Appl. Phys. **49**, 3276 (1978).
[29] T. S. Toellner, M. Y. Hu, G. Bortel, W. Sturhahn, and D. Shu, Nucl. Instrum. Methods Phys. Res. A **557**, 670 (2006).
[30] J. Lasave, F. Dominguez, S. Koval, M. G. Stachiotti, and R. L. Migoni, J. Phys.: Condens. Matter **17**, 7133 (2005).
[31] A. A. Maradudin, E. W. Montroll, G. H. Weiss, and I. P. Ipatova, *Theory of Lattice Dynamics in the Harmonic Approximation*, edited by H. Ehrenreich, F. Seitz, and D. Turnbull (Academic Press, New York, 1971), Chap. IV, p. 129.
[32] W. Sturhahn and A. Chumakov, Hyperfine Interact. **123/124**, 809 (1999).
[33] V. A. Bryukhanov, N. N. Delyagin, A. A. Opalenko, and V. S. Shpinel, Sov. Phys. JETP **16**, 310 (1963).
[34] W. Sturhahn and V. G. Kohn, Hyperfine Interact. **123/124**, 367 (1999); see in particular Eqs. (59)–(61) and Table I therein.
[35] M. Y. Hu, W. Sturhahn, T. S. Toellner, P. D. Mannheim, D. E. Brown, J. Zhao, and E. E. Alp, Phys. Rev. B **67**, 094304 (2003).
[36] H. R. Schoberr and P. H. Dederichs, in *Phonon States of Elements, Electron States and Fermi Surfaces of Alloys*, edited by K. H. Hellwege and J. L. Olsen, Landolt Börnstein, New Series II/13a (Springer, Berlin, 1981).
[37] H. Giefers, Ph.D. thesis, University of Paderborn, 2004.
[38] A. I. Chumakov, R. Rüffer, A. Q. R. Baron, H. Grünsteudel, H. F. Grünsteudel, and V. G. Kohn, Phys. Rev. B **56**, 10758 (1997).
[39] V. G. Kohn, A. I. Chumakov, and R. Rüffer, Phys. Rev. B **58**, 8437 (1998).